Central European Journal of Energetic Materials, **2015**, *12*(1), 129-144
ISSN 2353-1843

Controlled Synthesis and Application of Nano-energetic Materials Based on the Copper Oxide/Al System

Simin HE, Jin CHEN, Guangcheng YANG, Zhiqiang QIAO*, Jinshan LI*

Institute of Chemical Materials, China Academy of Engineering Physics, Mianyang 621900, China
** E-mail: ljshan245@163.com*

Abstract: Nanothermite composites containing metal oxide and metal fuel are attracting attention due to their outstanding combustion characteristics. The morphology of metal oxide is important for the performance of nanothermite composites. In this paper, branch-, plate-, sphere-, and hollow sphere-like CuO nano/microstructures were synthesized via a facile hydrothermal process. The CuO/Al based nanothermites were prepared via ultrasonic mixing of the as-obtained CuO products and nano-Al. The combustion behaviour of CuO/Al based nanothermites was analyzed by DSC and laser ignition. This study shows that this nanoscale mixing resulted in a large interfacial contact area and low diffusional resistance between the fuel and the oxidizer, and the reaction reflects large energy and laser ignition sensitivity.

Keywords: nanoenergetic material, CuO/Al, laser ignition, plate-like, hollow sphere

1 Introduction

As developing nanoenergetic materials (nEMs), nanothermites composed of metal oxide and metal fuel at the nanoscale have shown better performance in ignition and energy release [1-5], and promising applications have been proposed for clean primers and detonators, chemical neutralization agents, thermal batteries [6], IR flares/decoys [7], in-situ welding and soldering [8], rocket propellants and explosives [9], and nanoenergetics on a chip [10]. CuO/Al based nEMs are some of the fastest nanothermites with the highest exothermicity in combustion reaction

propagation. Al nanoparticles are one of most commonly used fuels due to their ready availability, fast oxidization kinetics [11], high energy density and reactivity [12-13]. The role of the oxygen species is not only as a strong oxidizer but also as an energy propagation medium that carries heat to neighboring particles [8]. The shape and surface area of nano/micro-sized CuO can dramatically affect the properties and performance [14]. The morphology of the nano-sized CuO influences the surface area and oxygen release [15]. This is important for the performance of CuO/Al-based nEMs. CuO/Al bilayer nanofoils, composed of a nanolayer of CuO and a nanolayer of Al [16], nanospheres [17], powders [3, 18-21], nanowires [7, 22-25] or nanorods [26-27] of CuO, mixed with nano/micro Al as CuO/Al nEMs have been widely studied. Few studies have focused on other shapes of CuO, such as branch, plate and so on. A recent report further confirms that hollow spherical CuO [28] shows enhanced performance in combustion behaviour, faster release of oxygen, and excellent gas-generation behaviour, associated with larger contact areas and shorter diffusion distances between nanosized Al and hollow CuO spheres.

Several methods have been developed to fabricate various CuO morphologies, including templating of colloidal particles, thermally annealing Cu film [19, 29], solvothermal methods using organic solvents, and physical deposition methods [3], *etc*. However, multistep processing, the required toxic raw materials, and the contamination of the byproducts has limited their exploitation. However, more facile and simple synthetic strategies should still be exploitable.

In the present work, we demonstrate a facile hydrothermal process for the controllable synthesis of branch-, plate-, sphere-, and hollow sphere-like nano/micro-sized CuO. Moreover, CuO/Al based nEMs were synthesized via ultrasonic mixing of the as-obtained CuO with nano-sized Al. Laser ignition experiments were performed for verifying the influence of these different morphologies on the nEMs. In addition, we have compared their energetic performance in terms of the energy release and the laser ignition energy of four CuO/Al composites. This interesting hierarchical structure exhibits significantly improved combustion performances, and not only maximizes the high heat of thermite reactions, but also has the advantage of a low ignition temperature.

2 Experimental

2.1 Materials

Cupric acetate hydrate ($Cu(OAc)_2 \cdot H_2O$, $Cu(OCOCH_3)_2 \cdot H_2O$) was purchased from Alfa Aesar Company. Ammonia, analytically pure, was obtained from

Tianjin Kemiou Chemical Reagent Co. Ltd. Al nanoparticles (size ~70 nm) were purchased from Sigma-Aldrich. Pure water was obtained from a Millipore Milli-Q system.

2.2 Synthesis of nano/micro-sized CuO

CuO nano/microstructures were synthesized via a hydrothermal process. A typical synthesis was as follows: $Cu(OAc)_2 \cdot H_2O$ (0.6 g) and a specified amount of ammonia were dissolved in pure water (30 mL), and the solution was stirred for 10 min. The solution was then transferred into a 50 mL stainless steel autoclave with a Teflon® liner and heated in an oven at 160 °C for 16 h. After cooling to room temperature, the resultant products were isolated via centrifugation and washed several times with pure water and ethanol. Finally, the products were dried in air at 80 °C for 3 h.

2.3 Characterization

The products were characterized via X-ray diffraction (XRD, Bruker D8 Advance diffractometer with Cu-Kα radiation (λ=1.5406 Å)). XRD was also used to ascertain any alteration in the phases present in the nanothermites before and after combustion. The particle size and morphology were visualized by field emission scanning electron microscopy (FESEM, Apollo 300) and high-resolution transmittal electronic microscopy (HRTEM, Libra 200). UV-spectra were characterized via an Hitachi U-3010 spectrophotometer. In conjunction with SEM imaging, energy-dispersive X-ray (EDX) microanalysis (Bruker AXS, Fitchburg, WI, USA) was performed to generate elemental maps.

2.4 Preparation of nanoenergetic composites

The CuO products were mixed with Al nanoparticles at a mass ratio of 1:0.25, and then dispersed in sufficient cyclohexane to make a thick paste. This slurry was then ultrasonicated for 30 min to ensure intimate mixing, the cyclohexane was allowed to evaporate off under ambient conditions, followed by a final drying step in an oven at 60 °C.

2.5 Thermal analysis and laser ignition

The heat of reaction of the CuO/Al nEMs was determined by thermogravimetric and differential scanning calorimetry (TGA-DSC, NETZSCH STA 449C). The experiment was performed from 30 to 1000 °C at a heating rate of 5 °C/min under 99.995% Ar flow.

The laser ignition test system was composed of a high stability Q-switched Nd:YAG pulse laser operating at 1064 nm, a power source and a related optical

system. A sketch of the laser ignition measurement system is shown in Figure 1. The laser voltage was 300 V, with a pulse width of 8 ns and pulse energies varying from 25 to 300 mJ, using a 70 mm condensing lens. The laser beam diameter was 1.5 mm. Composites were uncompacted into a solid cylinder with 4 mm diameter and length 2 mm.

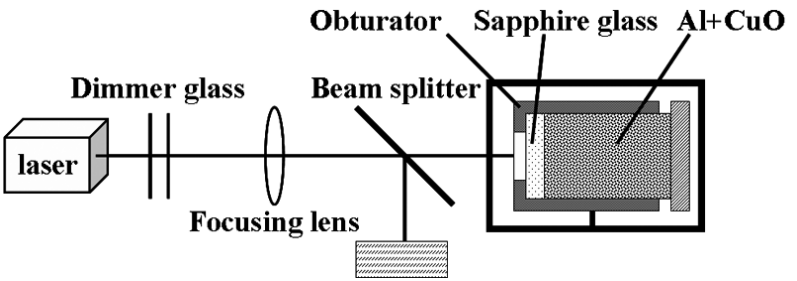

Figure 1. Schematic diagram of the laser ignition system.

3 Results and Discussion

3.1 Structure and Morphology

The morphologies of the as-synthesized CuO are as shown in Figure 2. Figure 2a shows the 3D branch-like nanostructures at an NH_4^+/Cu^{2+} ratio of 4. The branch-like CuO nanostructures consist of sub-branched nanorods with diameters of about 20-100 nm, which radiate from the sides of the main stem of the branch-like CuO nanostructures. Figure 2b shows that the plate-like CuO nanostructures have smooth surfaces with length ~300-400 nm and width ~100-200 nm. Moreover, the CuO spheres with diameters of 300-400 nm were formed when the NH_4^+/Cu^{2+} ratio was 2, as shown in Figure 2c. When the ratio was decreased to less than 1, the hollow spherical architecture ranged from 2 to 3 μm in diameter. A crushed microsphere vividly demonstrates a sphere wall with thickness 400 nm and consisting of many, mainly aggregated, pieces of small nanorods, as shown in Figure 2d. Figure 2e shows the typical XRD pattern of an as-prepared sample. It can be observed that all of the peaks in the diffraction pattern are consistent with the monoclinic phase of CuO (JCPDS 48-1548). No reflected peaks from other impurities are detected in the sample, which indicates the high purity of the as-obtained CuO products.

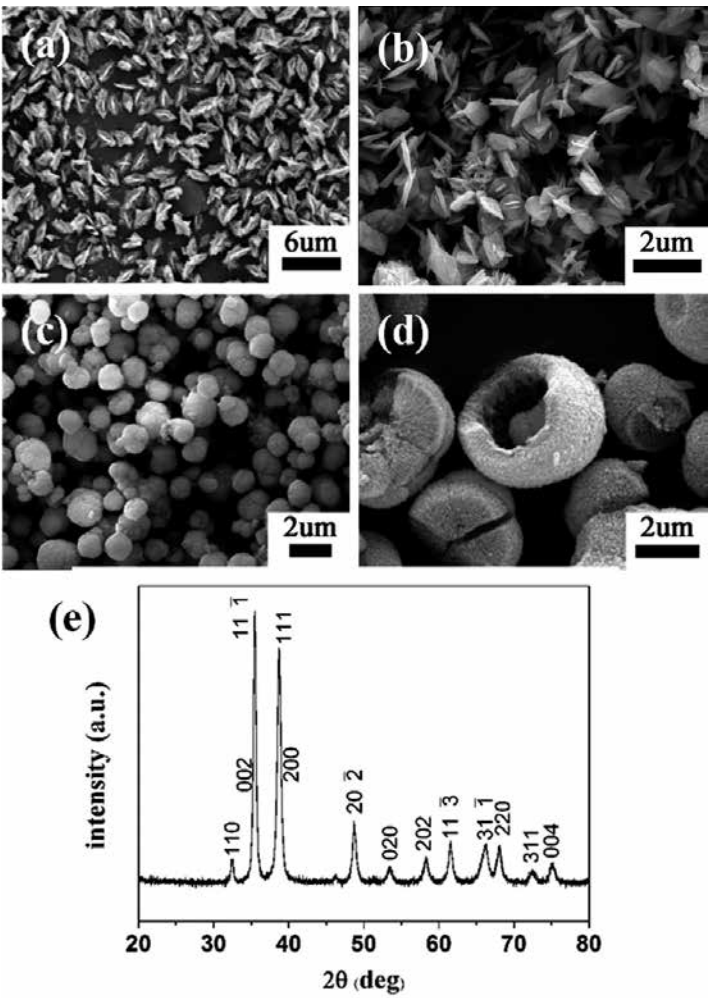

Figure 2. SEM images of (a) branch-, (b) plate-, (c) sphere- CuO, (d) hollow sphere-like CuO, and (e) a typical XRD pattern of the as-obtained CuO products.

The formation of CuO by the hydrothermal method using $Cu(OAc)_2 \cdot H_2O$ as the copper source has been studied in detail. These CuO nano/microstructures were formed through a process of self-assembly. In the present reaction system, the main chemical reactions in the aqueous solution can be formulated as follows:

$Cu(OCOCH_3)_2 \cdot H_2O + H_2O \rightarrow Cu^{2+} + 2CH_3COOH + 2OH^-$
$Cu^{2+} + 2OH^- \rightarrow Cu(OH)_2$
$Cu(OH)_2 \rightarrow CuO + H_2O$

Re-combination and joining between the precursor particles is destroyed to form ions or ionic groups in the solution, and then re-formed as grains at an early stage. The crystals grow freely, the growth habits of each crystal face being fully exposed under the hydrothermal conditions. Furthermore the growth of the crystals is unforced, so that the annexing agent significantly affect the crystal morphologies. Ammonia is a good precipitating agent, it can be used as a source of alkali, complexing agent or eroding agent under different conditions. It plays a crucial role in the synthesis of the CuO nanostructures. When the ammonia is added to the solution of $Cu(OAc)_2$, the following reactions occur:

$NH_3 \cdot H_2O \rightarrow NH_4^+ + OH^-$
$Cu^{2+} + 4NH_3 \rightarrow [Cu(NH_3)_4]^{2+}$
$[Cu(NH_3)_4]^{2+} + 2OH^- \rightarrow CuO + H_2O + 4NH_3$

A suggested morphology formation scheme for the CuO nano/microstructure is illustrated in Figure 3. Obviously, when ammonia is in excess, $[Cu(NH_3)_4]^{2+}$ is first generated by the reaction of $Cu(OAc)_2$ and ammonia [30], and has a sheet-like structure together with Cu^{2+} ions, and which then brakes down into CuO at high temperature. Therefore, as shown in route a, the product has a lamellar structure when the ratio of NH_4^+/Cu^{2+} is larger than 2. During the crystal growing period, high-index facets usually have fast growth rates, due to the high surface energy, and then subsequently disappear. The nanostructures, such as the branch-like type, with high-index facets could be obtained in high yields when controlled by excess ammonia as the alkali source. In route b, the bubbles of ammonia gas under high-temperature hydrolysis can rapidly provide OH^-, which then can act as a template together with Cu^{2+}, to precipitate the $Cu(OH)_2$ complexes almost at the same time [31]. The $Cu(OH)_2$ complexes maintain uniformity of particle size to a certain extent. When the hydrothermal reaction was carried out at a particular temperature, the newly-produced $Cu(OH)_2$ might be decomposed and completely converted to CuO by a dehydration reaction. Small nanoparticles might aggregate and crystallize around the surface of the bubbles. The OH^- could affect the morphology of the CuO nanostructures through adjustment of the interplanar H-bonds. With crystal growth and Ostward ripening [30], one could imagine that the bunched nanowires would interlink around the surface and form microspheres when the quantity of nanowires in the solution was large enough.

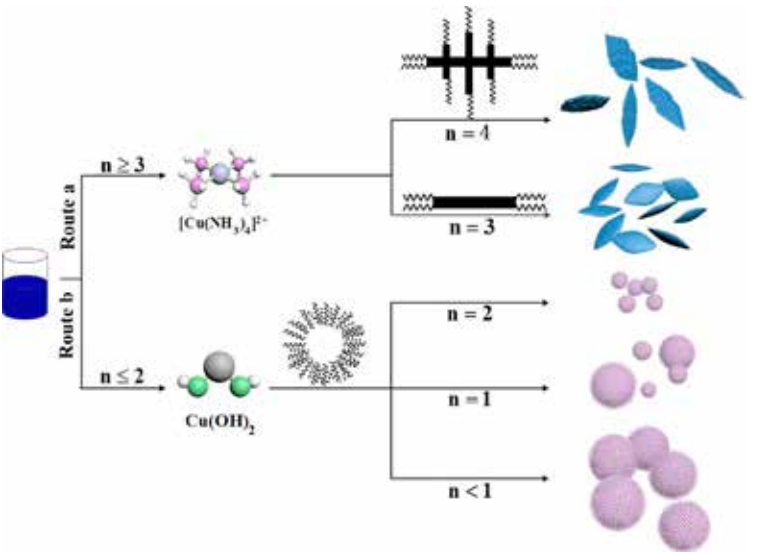

Figure 3. Schematic diagram of the effect of different proportions of ammonia in the synthesis of different morphologies of CuO; n is the molar ratio of NH_4^+/Cu^{2+}.

Clearly, the molar ratio of NH_4^+/Cu^{2+} is a crucial factor in the formation of the hierarchical CuO nano/microstructures. When the molar ratio of NH_4^+/Cu^{2+} is less than 1, the products are microspheres of diameter 1-2 μm, whilst when the molar ratio of NH_4^+/Cu^{2+} was equal to 1, the resulting products are a mixture of microspheres and nanospheres. Thus, an appropriate molar ratio of NH_4^+/Cu^{2+} may be favorable for the controlled synthesis of the CuO nano/microstructures. At the same time, it is easy to obtain hollow spheres during the process of sphere formation because of the etching by ammonia.

The thermal stability of the as-synthesized CuO nanostructure was studied via TGA and DSC simultaneously. Figure 4 shows the TGA-DSC curves of a sample. The weight loss during the temperature range is indicted by I, II, and III. I: the weight loss (1.28%) below 230 °C is ascribed to the removal of the physically adsorbed water; the presence of an endothermic DSC peak confirms the evaporation of water. II: the weight loss (3.80%) between 230 and 280 °C is assigned to the evaporation of intercalated water molecules; the exothermic DSC peak around 270 °C is consistent with the decomposition of residual polymer in the as-prepared CuO sample. These features are consistent with the TGA results [32-33]; III: the weight loss from 780 to 850 °C is associated with decomposition of CuO into Cu_2O ($4CuO \rightarrow 2Cu_2O + O_2$). Calculated weight

loss of 10%, due to incomplete decomposition, the actual weight loss is about 6.76%. No significant weight loss was observed between 280 and 780 °C, which indicates the thermal stability of the as-prepared CuO.

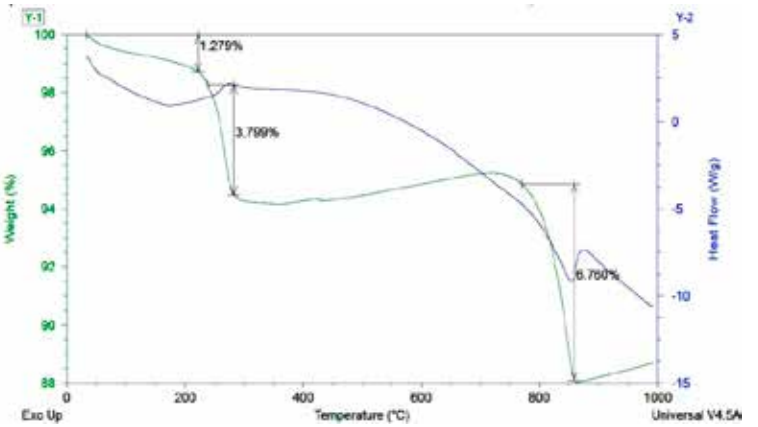

Figure 4. TGA/DSC plots of the as-produced CuO.

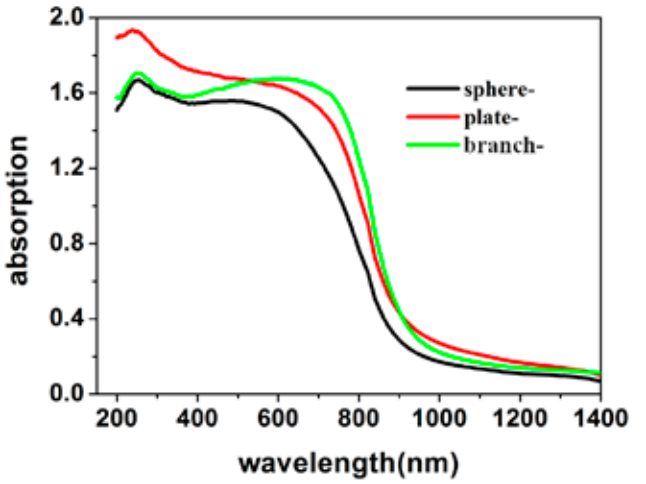

Figure 5. UV-Visible absorption spectra of the as-obtained CuO products**.**

3.2 UV-Visible Absorption Spectra

To determine the bandgap of the samples, the UV-visible absorption spectra of the as-prepared CuO products with different morphologies were obtained (Figure 5). The bandgap energy depends on the morphology of the CuO nanostructures [34-35]. Several obvious sharp peaks of branch-, plate- and sphere-like CuO were

identified at 250, 250, and 240 nm, respectively. The observed value is in good agreement with an earlier result [36], which is considerably blue-shifted from the value of 360 nm that was reported by Hong *et al.* [34] and 375 nm that was reported by Xu *et al*. [37]. The wavelength of the absorption edges (λg) was determined by extrapolating the horizontal and the sharply increasing portions of the curve to the abscissa at zero absorption [38]. The absorption edges of branch-, plate- and sphere-like CuO occur at 910, 900 and 860 nm, respectively. The energy bandgap of CuO was found using the following Equation:

$$E_g(eV) = \frac{1240}{\lambda g}$$

The bandgaps of the branch-, plate-, and sphere-like CuO products were estimated to be 1.36, 1.38 and 1.44 eV, respectively. The morphology of the CuO nanostructure significantly affects its bandgap. The well-known quantum confinement effects may have caused the blue-shift of the absorption peak and the increase in the bandgap. The observed blue-shift in the bandgap value, compared with the bulk CuO value, may be attributed to the quantum confinement effect, and the observed bandgap value is in good agreement with an earlier result [39].

3.3 Application in nEMs

The properties of energetic materials are known to be strongly influenced by the shape and surface area of nano/micro-sized CuO. Figure 6 shows the SEM images of ~70 nm Al particles mixed with three morphologies of CuO, and confirms that the as-produced CuO is completely covered with deposited Al. Thus good dispersive mixing, to ensure powder homogeneity, increasing the contact between fuel and oxidizer, is crucial for efficient and reliable combustion [40]. Therefore, by homogenizing the distribution of Al around the CuO, the rate of energy release can be substantially enhanced due to an increase in the contact area.

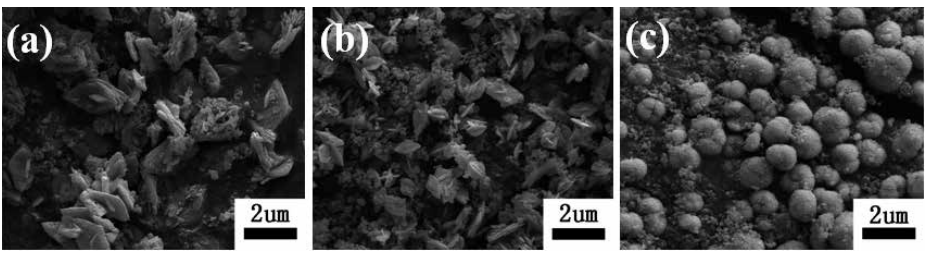

Figure 6. SEM images of (a) branch-, (b) plate-, (c) sphere-like CuO, mixed with ~70 nm Al particles.

Figure 7 shows the SEM and TEM images of hollow sphere-like CuO mixed with Al particles. After Al deposition, the average diameter of the microspheres was around 3 μm. Nano-Al is uniformly integrated around the CuO, thus enhancing the interfacial contact and reactivity. The reaction between CuO spheres and nano-Al can be complete and the heat energy can be released more effectively.

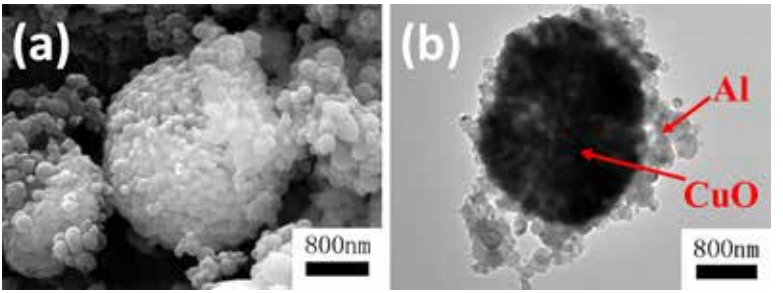

Figure 7. (a) SEM and (b) TEM images of hollow sphere-like CuO/Al.

As shown in Figure 8a, the EDX analysis comfirms the presence of Cu, Al, and O elements, with no other impurities. The compositions of the nEMs were further identifed by XRD, as shown in Figure 8b. Only Al and CuO diffraction lines can be seen in the XRD pattern. There are no peaks for Al_2O_3, Cu and Cu_2O, indicating that no signicant reaction between Al and CuO occurs. This reveals that this composite exhibits the characteristics of intermolecular composites (MIC).

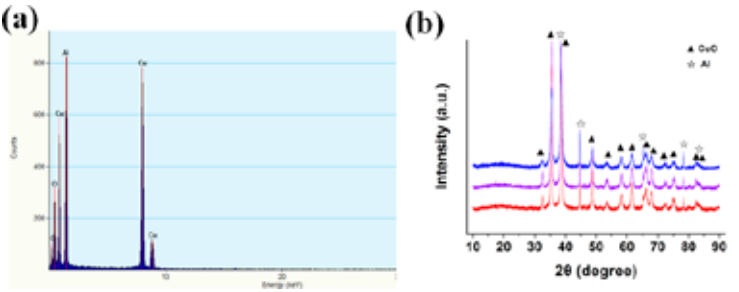

Figure 8. (a) EDX analysis and (b) XRD patterns of the CuO/Al based nEMs before reaction.

The CuO/Al powders were characterized by DSC to quantitatively determine the heat flow and onset temperature of the exothermic reactions (Figure 9). The heat flow profiles of Al with branch-, plate-, sphere-like CuO based nEMs are very similar, and are shown in Figure 9a. There are three major peaks

associated with the thermite reaction in each curve. The first (exothermic) peak, with an onset temperature at approximately 587 °C, is 433 °C lower than that of the microscale CuO/Al based nEMs (1040 °C) [7]. The reduced onset temperature is caused by the reaction between the CuO nano/microstructures and nanosized-Al based on the enhanced solid-solid diffusion mechanism [3, 19]. The low reaction temperature is very attractive for many applications that require energetic materials with low ignition temperatures, such as actuation, propulsion, power and so on. The second (endothermic) peak at 660 °C is caused by the melting of the remaining Al, thereby indicating that some Al nanopowder was still present after the thermite reaction. The peak near 800 °C probably corresponds to the dissolution of CuO in the Al melt [41]. The DSC plot of Al with hollow sphere-like CuO is shown in Figure 9b, the strong exothermic reaction, with a heat release equal to 1000 J/g, is higher than the 962.9 J/g that was reported by Kim *et al*. [22]. The heat release of the four morphologies of the CuO/Al based nEMs is shown in Table 1. The high heat release is promoted by the higher surface energy associated with the mesopores and micropores in the sphere shells. The performance of the compounds can be improved by adjusting the dimensions of the CuO powder and by adjusting the amount of Al to obtain a stoichiometric reaction [7].

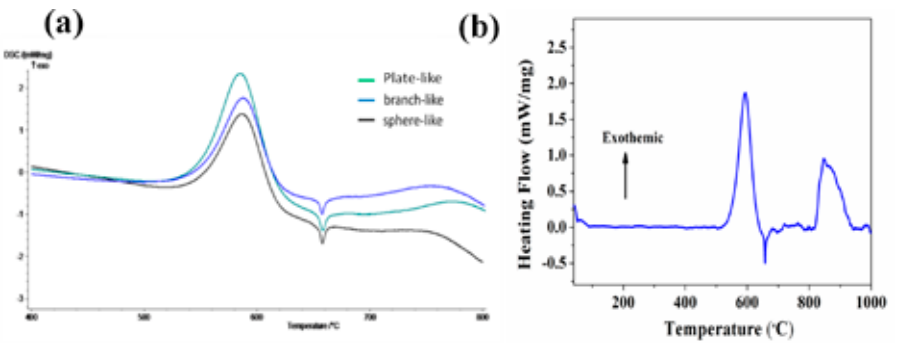

Figure 9. DSC plots of (a) Al with branch-, plate-, sphere-like CuO based nEMs, and (b) Al with hollow sphere-like CuO based nEMs.

Table 1. The heat released by the four morphologies of CuO/Al based nEMs

CuO morphology	Branch-like	Plate-like	Sphere-like	Hollow sphere-like
First onset temperature, [°C]	589	586	588	592
Heat released, [J/g]	879	890	831	1000

The ignitability of nEMs is an extremely important performance parameter. Compared to conventional electric spark ignition, laser ignition reduces emissions, gives faster ignition, and more stable combustion [42, 43], allowing the possibility of cavity ignition [44] and multi-point ignition [45]. Because thermite reactions are diffusion-controlled, decreasing the diffusion distance could potentially give decreased ignition times and increased reaction rates [3].

As Table 2 shows, the minimum laser ignition energy of the different morphologies is only 25 mJ, which confirms that the reflection coefficient is smaller than for micron-sized energetic materials. The laser energy required for ignition is dependent upon pre-ignition reactions, phase change/decomposition temperatures, confinement, and laser absorbance [46]. An early theoretical study showed that particle absorbance changes are based largely on particle size and that submicron metal particles absorb more energy than nanoparticles [47]. A loose powder mixture contains voids, producing gaps in the continuous flow of energy to form the thermal percolation network. Thermal percolation can cause "hot-spots" to form by the limited heat transfer away from the ignition zone [48]. Nano-sized particles can also reduce the oxygen release distance.

Table 2. The laser ignition energy of the four morphologies of CuO/Al based nEMs

Laser energy, [mJ]	25	40	70	140	200	250	300
Branch-like	×	×	√	√	√	√	√
Plate-like	√	√	√	√	√	√	√
Sphere-like	×	×	×	√	√	√	√
Hollow sphere-like	√	√	√	√	√	√	√

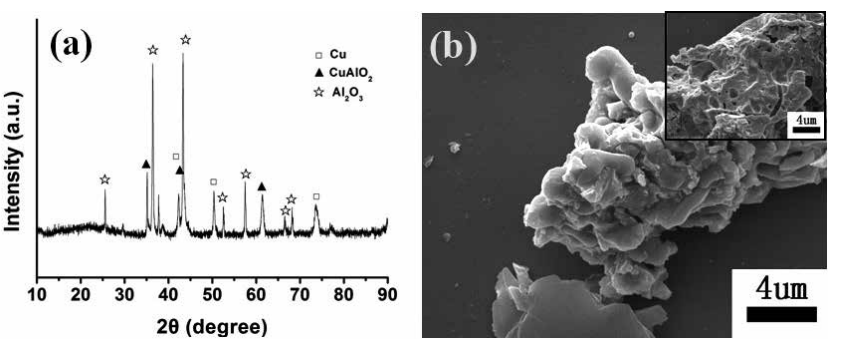

Figure 10. (a) XRD patterns of the CuO/Al based nEMs after reaction and (b) SEM image of the combustion products.

XRD confirmed that CuO was transformed into elemental Cu, while the Al was oxidized to Al_2O_3 after testing (as shown in Figure 10a). Figure 10b shows the SEM image of some of the combustion products. Great changes have taken place in the morphology of the product after combustion, due to the highly energetic impact of the combustion reaction between nano Al and CuO [3] and the high local temperature generated [11].

4 Conclusions

In summary, branch-, plate-, sphere-, and hollow sphere-like nano/micro-sized CuO have been successfully synthesized via a simple hydrothermal process by using cupric acetate as a reagent in the presence of ammonia. The performance of CuO/Al based nanothermite composites, prepared via ultrasonic mixing of the as-obtained CuO products with ~70 nm Al, is more effective as the interfacial area is substantially increased over conventional thermite composites. The higher combustion behaviour of hollow sphere- and nanoplate-like CuO based energetic composites can be attributed to a larger contact area and shorter diffusion distance as compared with the nanobranch-like CuO based composites.

Acknowledgments
This work was financially supported by the National Natural Science Foundation of China (11372288).

5 References

[1] Apperson S., Shende R.V., Subramaniaan S., Tappmeyer D., Gangopadhyay S., Generation of Fast Propagating Combustion and Shock Waves with Copper Oxide/ Aluminum Nanothermite Composites, *Appl. Phys. Lett.*, **2007**, *91*(24), 243109.
[2] Yetter R.A., Risha G.A., Son S.F., Metal Particle Combustion and Nanotechnology, *Proc. Combust. Inst.*, **2009**, *32*(2), 1819-1838.
[3] Granier J.J., Pantoya M.L., Laser Ignition of Nanocomposite Thermites, *Combust. Flame*, **2004**, *138*(4), 373-383.
[4] Song X., Wang J., Yang G.C., Nie F.D., Synthesis and Characterization of Al/CuO Nanothermite, *Chin. J. Energ. Mater.*, **2013**, *21*(1), 39-43.
[5] Feng J., Jian G., Liu Q., Zachariah M.R., Passivated Iodine Pentoxide Oxidizer for Potential Biocidal Nanoenergetic Applications, *ACS Appl. Mater. Interfaces*, **2013**, *5*, 8875-8880.
[6] Ohkura Y., Liu S., Rao P.M., Synthesis and Ignition of Energetic CuO/Al Core/

Shell Nanowires, *Proc. Combust. Inst.*, **2011**, *33*(2), 1909-1915.
[7] Koch E.C., 2006-2008 Annual Review on Aerial Infrared Decoy Flares, *Propellants Explos. Pyrotech.*, **2009**, *34*(1), 6-12.
[8] Shen J., Chan Y.C., Research Advances in Nano-composite Solders, *Microelectron. Reliab.*, **2009**, *49*(3), 223-234.
[9] Piercey D.G., Klapötke T.M., Nanoscale Aluminum-metal Oxide (Thermite) Reactions for Application in Energetic Materials, *Cent. Eur. J. Energ. Mater.*, **2010**, *7*(2), 115-129.
[10] Zhang K., Rossi C., Petrantoni M., Mauran N., A Nano Initiator Realized by Integrating Al/CuO-based Nanoenergetic Materials with a Au/Pt/Cr Microheater, *J. Microelectromech. Syst*., **2008**, *17*(4), 832-836.
[11] Yan S., Jian G., Zachariah M.R., Electrospun Nanofiber-based Thermite Textiles and Their Reactive Properties, *ACS Appl. Mater. Interfaces*, **2012**, *4*(12), 6432-6435.
[12] Wen D., Nanofuel as a Potential Secondary Energy Carrier, *Energ. Environ. Sci*., **2010**, *3*(5), 591-600.
[13] Jian G., Piekiel N.W., Zachariah M.R., Time-resolved Mass Spectrometry of Nano-Al and Nano-Al/CuO Thermite under Rapid Heating: a Mechanistic Study, *J. Phys. Chem. C*, **2012**, *116*(51), 26881-26887.
[14] He S.M., Li J.S., Wang J., Yang G.C., Qiao Z.Q., Facile Synthesis and Lithium Storage Performance of Hollow CuO Microspheres, *Mater. Lett.*, **2014**, *129*, 5-7.
[15] Zhou L., Piekiel N., Chowdhury S., Zachariah M.R., Time-resolved Mass Spectrometry of the Exothermic Reaction between Nanoaluminum and Metal Oxides: the Role of Oxygen Release, *J. Phys. Chem. C*, **2010**, *114*(33), 14269-14275.
[16] Kwon J., Ducéré J.M., Alphonse P., Bahrami M., Petrantoni M., Veyan J.F., Tenailleau C., Estève A., Rossi C., Chabal Y.J., Interfacial Chemistry in Al/CuO Reactive Nanomaterial and Its Role in Exothermic Reaction, *ACS Appl. Mater. Interfaces*, **2013**, *5*(3), 605-613.
[17] Kennedy A.J., Melby N.L., Moser R.D., Bednar A.J., Son S.F., Lounds C.D., Laird J.G., Nellums L.R., Johnson D.R., Steevens J.A., Fate and Toxicity of CuO Nanospheres and Nanorods Used in Al/CuO Nanothermites before and after Combustion, *Environ. Sci. Technol*., **2013**, *47*(19), 11258-11267.
[18] Stamatis D., Zhu X., Schoenitz M., Dreizin E.L., Redner P., Consolidation and Mechanical Properties of Reactive Nanocomposite Powders, *Powder Technol.*, **2011**, *208*, 637-642.
[19] Ermoline A., Stamatis D., Dreizin E.L., Low-temperature Exothermic Reactions in Fully Dense Al-CuO Nanocomposite Powders, *Thermochim. Acta*, **2012**, *527*, 52-58.
[20] Badiola C., Schoenitz M., Zhu X., Dreizin E.L., Nanocomposite Thermite Powders Prepared by Cryomilling, *J. Alloy. Compd.*, **2009**, *488*(1), 386-391.
[21] Wang H.Y., Jian G.Q., Egan G.C., Zachariah M.R., Assembly and Reactive Properties of Al/CuO Based Nanothermite Microparticles, *Combust. Flame*, **2014**, *161*, 2203-2208.
[22] Kim D.K., Bae J.H., Kang M.K., Kim H.J., Analysis on Thermite Reactions of

CuO Nanowires and Nanopowders Coated with Al, *Curr. Appl. Phys.*, **2011**, *11*, 1067-1070.
[23] Zhang K., Rossi C., Ardila Rodriguez G.A., Development of a Nano-Al/CuO Based Energetic Material on Silicon Substrate, *Appl. Phys. Lett.*, **2007**, *91*(11), 113117.
[24] Sullivan K., Young G., Zachariah M.R., Enhanced Reactivity of Nano-B/Al/CuO MIC's, *Combust. Flame*, **2009**, *156*(2), 302-309.
[25] Petrantoni M., Rossi C., Conédéra V., Bourrier D., Alphonse P., Tenailleau C., Synthesis Process of Nanowired Al/CuO Thermite, *J. Phys. Chem. Solids*, **2010**, *71*, 80-83.
[26] Shende R., Subramanian S., Hasan S., Apperson S., Thiruvengadathan R., Gangopadhyay K., Gangopadhyay S., Nanoenergetic Composites of CuO Nanorods, Nanowires, and Al-nanoparticles, *Propellants Explos. Pyrotech.*, **2008**, *33*(2), 122-130.
[27] Sanders V.E., Asay B.W., Foley T.J., Tappan B.C., Pacheco A.N., Son S.F., Reaction Propagation of Four Nanoscale Energetic Composites (Al/MoO_3, Al/WO_3, Al/CuO, and Bi_2O_3), *J. Propul. Power*, **2007**, *23*(4), 707-714.
[28] Jian G., Liu L., Zachariah M.R., Facile Aerosol Route to Hollow CuO Spheres and Its Superior Performance as an Oxidizer in Nanoenergetic Gas Generators, *Adv. Funct. Mater.*, **2013**, *23*, 1341-1346.
[29] Zhang K., Rossi C., Tenailleau C., Alphonse P., Chane-Ching J.Y., Synthesis of Large-area and Aligned Copper Oxide Nanowires from Copper Thin Film on Silicon Substrate, *Nanotechnology*, **2007**, *18*(27), 275607.
[30] Qin Y., Zhang F., Chen Y., Zhou Y., Zhu A., Luo Y., Tian Y., Yang J., Hierarchically Porous CuO Hollow Spheres Fabricated via a One-pot Template-free Method for High-performance Gas Sensors, *J. Phys. Chem. C*, **2012**, *116*, 11994-12000.
[31] Zhang X., Wang G., Liu X., Wu J.J., Li M., Gu J., Liu H., Fang B., Different CuO Nanostructures: Synthesis, Characterization, and Applications for Glucose Sensors, *J. Phys. Chem. C*, **2008**, *112*(43), 16845-16849.
[32] Zhang Y.X., Huang M., Kuang M., Liu C.P., Tan J.L., Dong M., Yuan Y., Zhao X.L., Wen Z., Facile Synthesis of Mesoporous CuO Nanoribbons for Electrochemical Capacitors Applications, *Int. J. Electrochem. Sci.*, **2013**, *8*, 1366-1381.
[33] Singh I., Bedi R.K., Surfactant-assisted Synthesis, Characterizations, and Room Temperature Ammonia Sensing Mechanism of Nanocrystalline CuO, *Solid State Sci.*, **2011**, *13*(11), 2011-2018.
[34] Hong J., Li J., Ni Y., Urchin-like CuO Microspheres: Synthesis, Characterization, and Properties, *J. Alloy. Compd.*, **2009**, *481*(1), 610-615.
[35] Xiao H.M., Fu S.Y., Zhu L.P., Li Y.Q., Yang G., Controlled Synthesis and Characterization of CuO Nanostructures through a Facile Hydrothermal Route in the Presence of Sodium Citrate, *Eur. J. Inorg. Chem.*, **2007**, *14*, 1966-1971.
[36] Shao Q., Wang L., Wang X., Yang M., Ge S., Yang X. Wang J., Hydrothermal Synthesis and Photocatalytic Property of Porous CuO Hollow Microspheres via PS Latex as Templates, *Solid State Sci.*, **2013**, *20*, 29-35.
[37] Xu X., Zhang M., Feng J., Zhang M., Shape-controlled Synthesis of Single-

crystalline Cupric Oxide by Microwave Heating Using an Ionic Liquid, *Mater. Lett.*, **2008**, *62*(17), 2787-2790.

[38] Wang J., Fan X.M., Wu D.Z., Dai J., Liu H., Liu H.R., Zhou Z.W., Fabrication of CuO/T-ZnOw Nanocomposites using Photo-deposition and Their Photocatalytic Property, *Appl. Surf. Sci.*, **2011**, *258*(5), 1797-1805.

[39] Yang M., He J., Fine Tuning of the Morphology of Copper Oxide Nanostructures and Their Application in Ambient Degradation of Methylene Blue, *J. Colloid Interf. Sci.*, **2011**, *355*(1), 15-22.

[40] Chen C., Yu C., Two-dimensional Image Characterization of Powder Mixing and its Effects on the Solid-state Reactions, *Mater. Chem. Phys.*, **2004**, *85*(1), 227-237.

[41] Ilunga K., Del Fabbro O., Yapi L., Focke W.W., The Effect of Si-Bi_2O_3 on the Ignition of the Al-CuO Thermite, *Powder Technol.*, **2011**, *205*(1), 97-102.

[42] Srivastava D.K., Weinrotter M., Iskra K., Agarwal A.K., Wintner E., Characterisation of Laser Ignition in Hydrogen-air Mixtures in a Combustion Bomb, *Int. J. Hydrogen Energ.*, **2009**, *34*(5), 2475-2482.

[43] Mullett J.D., Dodd R., Williams C.J., Triantos G., Dearden G., Shenton A.T., Watkins K.G., Carroll S.D., Scarisbrick A.D., Keen S., The Influence of Beam Energy, Mode and Focal Length on the Control of Laser Ignition in an Internal Combustion Engine, *J. Phys. D: Appl. Phys.*, **2007**, *40*(15), 4730-4739.

[44] Morsy M.H., Review and Recent Developments of Laser Ignition for Internal Combustion Engines Applications, *Renewable Sustainable Energy Rev.*, **2012**, *16*(7), 4849-4875.

[45] Weinrotter M., Iskra K., Al-Janabi A.H., Kopecek H., Wintner E., Laser Ignition of Engines: Multipoint, Fiber Delivery, and Diagnostics, *21st European Mask and Lithography Conference*, **2005**, 88-99.

[46] Stacy S.C., Pantoya M.L., Laser Ignition of Nano-composite Energetic Loose Powders, *Propellants Explos. Pyrotech.*, **2013**, *38*(3), 441-447.

[47] Qiu T.Q., Longtin J.P., Tien C.L., Characteristics of Radiation Absorption in Metallic Particles, *J. Heat Transfer*, **1995**, *117*(2), 340-345.

[48] Rashkovskii S.A., Hot-spot Combustion of Heterogeneous Condensed Mixtures, Thermal Percolation, *Combust., Explos. Shock Waves (Engl. Transl.)*, **2005**, *41*(1), 35-46.